Photodissociation of the propargyl and propynyl (C_3D_3) radicals at 248 nm and 193 nm

Paul E. Crider, Luca Castiglioni, Kathryn E. Kautzman,[a] and Daniel M. Neumark[b]

Department of Chemistry, University of California, Berkeley, California 94720, USA and Chemical Sciences Division, Lawrence Berkeley National Laboratory, Berkeley, California 94720, USA

Abstract

The photodissociation of perdeuterated propargyl (D_2CCCD) and propynyl (D_3CCC) radicals was investigated using fast beam photofragment translational spectroscopy. Radicals were produced from their respective anions by photodetachment at 540 nm and 450 nm (below and above the electron affinity of propynyl). The radicals were then photodissociated by 248 nm or 193 nm light. The recoiling photofragments were detected in coincidence with a time- and position-sensitive detector. Three channels were observed: D_2 loss, $CD + C_2D_2$, and $CD_3 + C_2$. Observation of the D loss channel was incompatible with this experiment and was not attempted. Our translational energy distributions for D_2 loss peaked at nonzero translational energy, consistent with ground state dissociation over small (<1 eV) exit barriers with respect to separated products. Translational energy distributions for the two heavy channels peaked near zero kinetic energy, indicating dissociation on the ground state in the absence of exit barriers.

[a] Current Address: California Institute of Technology, 1200 E. California Blvd., Pasadena, CA 91125

[b] Corresponding author. Email: dneumark@berkeley.edu

I. Introduction

C_3H_3 radicals have been of interest for decades owing to their importance in combustion and interstellar chemistry.[1-11] Of the various stable C_3H_3 isomers, propargyl (2-propynyl, H_2CCCH) has received the most attention. This is in part because propargyl lies over 30 kcal/mol below the other C_3H_3 isomers. The propargyl radical is resonance-stabilized, and is thus expected to accumulate in hydrocarbon flames.[12-15] It is now widely thought that the propargyl self-reaction forms the first benzene ring in combustion, as proposed by Wu and Kern.[1] Subsequent reactions with the benzene ring lead to the formation of polycyclic aromatic hydrocarbons (PAHs) and ultimately soot.[1-4,8-10,15,16] Due to its participation in atom-radical and radical-radical reactions without entrance barriers, the propargyl radical is also expected to be important in the chemistry of hydrocarbon-rich planetary atmospheres.[5,11] In this paper, we investigate the photodissociation dynamics of both the propargyl radical and the higher-lying 1-propynyl isomer, H_3CCC, at 248 nm and 193 nm using fast beam photofragment translational spectroscopy.

There have been numerous experimental and theoretical studies of the propargyl radical. Microwave[17] and infrared[18,19] spectroscopy have addressed the structure and vibrational frequencies of its ground electronic state. Its electron affinity (EA)[20-24] and ionization potential (IP)[23,25-28] have been determined. UV absorption studies[29-31] have probed the excited states of the radical, particularly an absorption band around 240 nm, assigned to the $\tilde{B}^2B_1 \leftarrow \tilde{X}^2B_1$ transition by Fahr *et al.*[30] Theoretical work has focused on the structure and thermochemistry of propargyl[13-15,28,32-34] as well as its role as an intermediate in small hydrocarbon reactions.[15,35-38]

The photodissociation of propargyl was first observed by Jackson *et al.* as secondary photodissociation from the photolysis of allene.[39] Jackson reported three dissociation channels: H loss, H_2 loss, and CH loss, with only minor contribution from the latter two channels. The H loss channel has subsequently been observed in radical photodissociation experiments by Deyerl *et al.*[40] and Goncher *et al.*[41] at 242 nm and 248 nm, respectively. McCunn *et al.*[42] observed this channel from the secondary photodissociation from propargyl chloride at 157 nm. The translational energy distributions obtained from studies suggested that H loss dissociation proceeds through a loose transition state following internal conversion to the ground state. Goncher *et al.*[41] and McCunn *et al.*[42] also observed H_2 loss; their results implied dissociation on the ground electronic state over an exit barrier of around 10 kcal/mol.

High-level calculations performed by Nguyen *et al.*[38] followed by a Rice-Ramsperger-Kassel-Marcus (RRKM) rate-constant analysis[43] identified the same three product channels at 193 nm and 242 nm and yielded branching ratios that agreed well with experimental values, though there was some disagreement as to whether the primary C_3H_2 fragment is cyclic. Eisfeld recently performed calculations[28,34] on the absorption spectrum of propargyl that questioned the assignment of 240 nm absorption to propargyl. Those calculations indicated that the absorption at 240 nm was dipole-forbidden and that the $\tilde{B}^2B_1 \leftarrow \tilde{X}^2B_1$ transition had a maximum around 220 nm, a value too high to be consistent with experiments. However, the recent photodissociation experiments by Goncher *et al.*[41] supported the original assignment of the 240 nm band.

Although it is also expected to be present in combustion, the propynyl radical, calculated to lie 41.9 kcal/mol above propargyl,[15] has been considerably more resistant to experimental characterization. Several experiments involving propynyl have sought to answer whether the

primary product of the photodissociation of propyne at 193 nm is propynyl or propargyl. Early experiments in the 1960s[29,44] suggested propargyl was the major photoproduct, but later studies[36,45-47] indicated propynyl. The most recent studies[48-53] confirm the earlier finding that propargyl is the major photoproduct formed by a statistical dissociation on the ground electronic state following internal conversion. One method that has proved effective for studying propynyl is anion photoelectron spectroscopy. This is because the propargyl and propynyl anions are nearly isoenergetic[22] while the radicals have very different electron affinities (0.918 eV and 2.735 eV, respectively[22,23]), making discrimination between the two species possible. The EA of 2.718 eV for propynyl was originally determined by anion photoelectron spectroscopy[21] and recently improved to 2.735 eV by higher resolution slow-electron velocity map imaging.[54] Theoretical approaches have yielded similar values.[22,23]

Theoretical work with propynyl has been primarily concerned with its thermochemistry and isomerization pathways.[15,35-38] Vibronic interactions between the ground electronic state ($^2A_1$) and the extremely low-lying first excited state (^2E, 3260 cm^{-1})[28] of propynyl cause artificial symmetry breaking in single-reference methods, making investigation of the excited states difficult. The only study to investigate the higher electronic excited states of propynyl explicitly was carried out by Eisfeld,[28] who predicted an energy gap between the first and second excited electronic states of propynyl just shy of 7 eV. This value is unusually large for an open shell species and appears inconsistent with the results presented in this paper.

The present work examines the photodissociation dynamics of both propargyl and propynyl at 248 nm and 193 nm by fast beam photofragment translational spectroscopy. Figure 1 shows an energy level diagram of the propargyl and propynyl isomers, their respective anions, and the accessible photodissociation channels along with arrows representing the dissociation

laser wavelengths. The values given in Figure 1 for H loss, H_2 loss, and the CH_3 loss channels were calculated from the heats of formation given by Nguyen *et al.*[38] and represent contributions from theory and experiment. The energy of the $CH + C_2H_2$ asymptote was taken from the ion-molecule thermochemical cycle reported by Robinson *et al.*[21] The change in enthalpy for the isomerization between the two neutral radicals was provided by Nguyen[38] and the barrier height was calculated by Vereecken *et al.*[37] The anion energetics were calculated by Ikuta.[22]

The propargyl and propynyl radicals of this study are prepared by photodetachment of their respective anions. The near degeneracy of the anions allows us to obtain additional information about the dissociation of the propargyl radical while simultaneously observing propynyl photodissociation for the first time. The present study is complementary to previous photodissociation studies[39-42] in that we are better equipped to detect the heavy mass channels but unable to detect H loss because our experimental set-up requires product mass ratios less than about 10:1 as described below. For the same reason, all experiments described in this work were performed on the fully deuterated C_3D_3 species and 'propargyl' and 'propynyl' will henceforth refer to their respective perdeuterated isotopologs. We confirm the presence of CD loss and D_2 loss channels from the propargyl radical at 248 and 193 nm. We also find that propynyl undergoes D_2 loss at 248 nm and dissociation to $CD_3 + C_2$ at both wavelengths. At 193 nm, this channel is also seen for propargyl.

II. Experimental

The fast beam photofragment translational spectrometer used in this study has been described in detail elsewhere.[55-57] Briefly, a pulsed, mass-selected beam of anions is photodetached by a laser pulse to produce a beam of the neutral radicals of interest. The neutrals

are photodissociated by a second laser, and the recoiling photofragments are detected in coincidence by a time- and position-sensitive detector. The information collected here is used to determine photofragment translational energy distributions ($P(E_T)$ distributions).

$C_3D_3^-$ ions were produced by supersonically expanding a 50 psi gas mixture of 10% NF_3 in argon seeded with 1-trimethylsilylpropyne-d_3 into a vacuum chamber with a piezoelectric valve pulsed at 60 Hz. 1-trimethylsilylpropyne (Aldrich, 99%) was used as received and deuterated by standard methods.[58] The pulsed jet expansion passed through an electrical discharge and intersected an electron beam. Propynyl anions were preferentially produced over propargyl due to the strong silicon-fluorine bond.[59] Nonetheless, as shown below, some propargyl anions were produced by isomerization in the ionization region.

The ions were collimated by a skimmer, accelerated to a beam energy of 6 keV, and then separated by mass by a Bakker time-of-flight mass spectrometer.[60,61] The ion packet was intercepted by a pulse from a XeCl excimer-pumped dye laser (Lambda-Physik LPX-200, Lambda-Physik FL 3000). This laser pulse photodetached some of the ions, and the remaining ions were deflected from the beam path, leaving a fast beam of neutral C_3D_3 radicals. Two laser wavelengths were used for photodetachment: 540 nm (2.30 eV) and 450 nm (2.76 eV). These wavelengths correspond to energies well below and just above the EA of propynyl-d_3 (2.735 eV);[54] both wavelengths are far above the electron affinity of propargyl-d_3 (0.915 eV)[21] but not energetic enough to access the first excited state of propargyl.[28,32,34,38] The C_3D_3 neutrals were then intercepted by a pulse from a second excimer laser (GAM EX-50F) operating at either 248 nm or 193 nm. This second pulse dissociated the radicals and the recoiling photofragments collided with the time- and position-sensitive detector 2.15 m downstream while the

undissociated parent beam impinged upon a 5 × 8 mm^2 beam block immediately in front of the detector.

The coincidence imaging detector consists of 75 mm diameter microchannel plates (MCPs) mounted in a Z-stack configuration and coupled to a phosphor screen.[56,57] The image from the phosphor screen was split by a dichroic beam splitter with the reflected image going to a 4 × 4 multianode photomultiplier tube (PMT) array and the transmitted fraction proceeding to an image intensifier in front of a charge-coupled device (CCD) camera. The arrival times of the photofragments were acquired by the PMT and were correlated with position information from the CCD camera. Only events where two photofragments struck within the same time window and the position information from the CCD matched the rough position information from the PMT were accepted. The coincident photofragment arrival time and position information was used to infer the photofragment masses and translational energy release for each dissociation event; from this data, the center-of-mass $P(E_T)$ distribution is constructed for each product channel.

III. Results and analysis

A. Photofragment identification

Because our primary method of identifying and separating the molecule of interest in the beam is by mass-selection and propargyl and propynyl are isomeric, it was necessary to ensure that propynyl was actually being produced. Figure 2 shows a plot of MCP signal intensity for photodetachment laser energies above and below the EA of propynyl. This plot corresponds to a photodetachment efficiency curve and the sharp increase at the point of the propynyl EA indicates that propynyl was indeed produced. However, there is nonzero signal below the

propynyl EA that must arise from photodetachment of the propargyl anion. Based on the photodetachment signal, the ratio of propynyl to propargyl above the propynyl EA is approximately 2 to 1.

Figure 3 shows the mass distributions for experiments performed at a dissociation laser wavelength of 248 nm. At a detachment laser wavelength of 540 nm (Fig. 3A), where only propargyl should be present, the observed photofragment masses correspond to D_2 loss and CD loss channels. The mass ratio of photofragments in the D loss channel is too large for both fragments to be detected simultaneously and that channel thus remains unobserved throughout this study. At 450 nm detachment (Fig. 3B), where propynyl is the major contributor, D_2 loss and CD loss are still observed, and a third channel corresponding to $CD_3 + C_2$ becomes evident, which must arise from propynyl photodissociation. The contribution from the CD_3 loss channel relative to CD loss is 0.7:1, despite the greater population of propynyl in the beam.

The mass distributions presented in Figure 4 are from experiments performed at a dissociation laser wavelength of 193 nm. At 540 nm detachment (Fig. 4A), D_2 loss and CD loss are again apparent, though the contribution from D_2 loss is diminished in comparison. There is also evidence for CD_3 loss. Photodetachment at 450 nm produces the same mass channels, but the relative contribution of CD_3 loss to CD loss increases from 0.7:1 to 1.8:1. Hence, at 193 nm, propargyl dissociates mainly by CD loss with a small contribution from CD_3 loss, while CD_3 loss is the main channel for propynyl.

B. Photofragment translational energy distributions

After the photofragment masses have been determined, the center-of-mass photofragment translational energy distributions ($P(E_T)$) are constructed from the coincidence data for each

product channel. Because of the presence of the beam block in the center of the detector and the finite radius of the MCPs, certain photodissociation events are detected with less efficiency than others and some events will not be detected at all. In order to correct for this, a detector acceptance function (DAF)[62] constructed from geometric parameters of the experiment is used to normalize the raw $P(E_T)$ distributions. With the exception of the D_2 loss channels, every product channel in every data set produced a $P(E_T)$ distribution sharply peaked at exactly zero E_T when normalized by the DAF. We suspect this peak at zero is an artifact of false coincidence events detected from the highly populated D loss channel. C_3D_2 fragments clustering around the beam block could be incorrectly assigned as momentum-matched fragments from the CD loss or CD_3 loss channels. This problematic effect is somewhat mitigated by discriminating fragments falling near the calculated center of dissociation, but normalization by the DAF still leads to $P(E_T)$ distributions that blow up at $E_T = 0$. Figure 5 shows a sample comparison of the normalized and raw $P(E_T)$ distributions calculated from identical data. Because DAF normalization only changes the shape of the $P(E_T)$ distributions at low E_T and leaves higher E_T events essentially unaltered, we have chosen to present the raw $P(E_T)$ distributions throughout the study. With the exception of the D_2 loss channels, which remain DAF normalized and un-discriminated, all $P(E_T)$ distributions were constructed from events where photofragments struck the detector within 6 mm of the calculated center of dissociation. This procedure discriminates against low kinetic energy events, especially those below about 150 meV, so our reported $P(E_T)$ distributions should be treated as speculative in that energy range.

Figure 6A shows the $P(E_T)$ distributions for D_2 loss at a dissociation laser wavelength of 248 nm. The red $P(E_T)$ distribution results from 540 nm detachment and thus represents only propargyl radicals while the black distribution results from 450 nm detachment, where propynyl

contributes. The propargyl $P(E_T)$ distribution peaks between 0.6 and 0.8 eV (14-18.5 kcal/mol). The 450 nm $P(E_T)$ distribution has a shoulder around 0.4 to 0.7 eV (9-16 kcal/mol) and a sharper peak around 0.8 eV (18.5 kcal/mol). The peak beginning around 0.7 eV is shifted to slightly higher E_T than the peak in the propargyl distribution and thus must be due to the presence of propynyl. Though D_2 loss was evident at 193 nm, there was not enough signal to construct a meaningful $P(E_T)$ distribution.

Figure 6B presents a comparison of the 248 nm propargyl photodissociation results from this study (in red) with the work of Goncher *et al,* shown in black.[41] Note that the $P(E_T)$ distributions from Goncher's study are constructed by a forward convolution fit to experimental time-of-flight distributions. The results from the two different methods are in reasonable agreement.

Figure 7 presents the $P(E_T)$ distributions for the CD + C_2D_2 channel and compares them holding either the photodetachment wavelength or the photodissociation wavelength constant. All of the $P(E_T)$ distributions peak close to zero kinetic energy release and extend to approximately 1.25 eV. Figures 7A and 7B show that at either dissociation wavelength, the $P(E_T)$ distributions are similar for 540 nm and 450 nm detachment. The energy level diagram in Figure 1 indicates that the CD + C_2D_2 channel is accessible by both isomers in each of these experiments. Figures 7C and 7D show that at both detachment wavelengths, the 193 nm $P(E_T)$ distribution shifts slightly further away from zero E_T compared to the 248 nm distribution. However, no dependence on photodissociation laser wavelength is evident for $E_T > 1.0$ eV.

The $P(E_T)$ distributions for the CD_3 + C_2 channel at 193 nm are presented in Figure 8. In contrast to the situation for the CD + C_2D_2 channel, these distributions depend on the

photodetachment wavelength. Both $P(E_T)$ distributions for the CD_3 loss channel peak close to $E_T = 0$. CD_3 and C_2 products were observed in the 540 nm/193 nm experiment, where only propargyl radicals should be present in the beam. In the experiment with 450 nm detachment, where propynyl is dominant, the $P(E_T)$ distribution (Fig. 6, black) also peaks near zero E_T, but is more heavily weighted to higher translational energy than the propargyl distribution.

IV. Discussion

In the $P(E_T)$ distributions discussed in this report, the translational energy is given by

$$E_T = h\nu + E_{int} - E_{frag} - D_0, \quad (1)$$

where $h\nu$ is the dissociation photon, E_{int} is the internal energy of the parent radical, E_{frag} is the internal energy of the photofragments, and D_0 is the dissociation energy. The internal energy of the anions is assumed to be zero in these experiments. Note that, while neutral propynyl is produced in its vibrational ground state upon photodetachment, neutral propargyl is vibrationally excited. At either detachment wavelength, a significant portion of the Franck-Condon profile of the propargyl anion photoelectron spectrum is accessible, covering electron binding energies from 0.919 to 1.9 eV,[21] so the propargyl radicals can have up to 1 eV of internal energy. The maximum energy available for translation ($E_{T,max}$) is then given by

$$E_{T,max} = h\nu + E_{int} - D_0, \quad (2)$$

where E_{int} is 1 eV in the case of propargyl and 0 for propynyl and no available energy is deposited into internal degrees of freedom of the recoiling photofragments. The arrows in Figure 1 illustrate the channels that can be accessed by 248 nm (red) and 193 nm (blue) dissociation laser wavelengths, with the dashed continuations representing the additional energy from

photodetachment available for propargyl. Table 1 lists the values of $E_{T,\,max}$ in eV, calculated from the values given in Figure 1.

Figure 1 thus shows that with the additional internal energy gained from photodetachment, propargyl can dissociate to CH + C_2H_2 at 248 nm and, at 193 nm, to CH_3 + C_2 as well. Cold propynyl radicals can dissociate to both channels at both wavelengths, but the CH_3 + C_2 channel is barely accessible at 248 nm, with only 0.1 eV of energy available.

The remainder of the discussion is separated into three sections, according to product channel. Sections A, B, and C will respectively discuss D_2 loss, CD + C_2D_2, and CD_3 + C_2. Each section will discuss that product channel in terms of both photodetachment and photodissociation laser wavelengths and the possible pathways to dissociation for each isomer.

A. D_2 + C_3D

The major motivation for this work was to investigate the dynamics of the heavy product channels of propargyl and propynyl photodissociation. Though the mass ratio of photofragments for D_2 loss (9.5:1) is at the very edge of the geometric limitations of our experiment, we were able to detect this channel and construct limited $P(E_T)$ distributions. Figure 6A shows $P(E_T)$ distributions for D_2 loss from propargyl (red) and propynyl (black) at 248 nm. In the propargyl distribution, the onset of the peak around 0.4 eV is close to the calculated barrier height[38] of 0.44 kcal/mol. The onset of the peak in the $P(E_T)$ distribution for propynyl near 0.7 eV (14 to 16 kcal/mol) also agrees with the 16.4 kcal/mol barrier height for that channel calculated by Nguyen. Both $P(E_T)$ distributions for D_2 loss thus peak near the exit barrier height, which is consistent with statistical dissociation over a late barrier.[38] Figure 6B compares the $P(E_T)$

distribution for D_2 loss with that reported by Goncher and shows reasonable agreement in the region of most intensity from 0.4 to 0.9 eV (9 to 21 kcal/mol).

B. CD + C_2D_2

The CD + C_2D_2 channel was observed in every experiment performed (Figures 3 and 4). $P(E_T)$ distributions are compared by photodetachment wavelength in Figures 7A and 7B. The similarity of the distributions at either photodissociation wavelength with photodetachment energies above and below the EA of propynyl suggests that propargyl is the major contributor to this dissociation pathway. When propynyl is present, there is enough available energy to access this channel via isomerization to propargyl, but our experiment offers no compelling evidence that this occurs.

Each $P(E_T)$ distribution extends to around 1.4 eV, lower than the $E_{T,\,max}$ values expected from Table 1, indicating the available energy is retained in internal modes. Figures 7C and 7D compare the $P(E_T)$ distributions by dissociation wavelength at either detachment wavelength. At either detachment wavelength, the average E_T increased as the dissociation laser energy increased. At 540 nm detachment, the average E_T increases from 0.30 ± 0.02 eV to 0.40 ± 0.02 eV going from 248 nm to 193 nm. For 450 nm detachment, the average E_T increases from 0.33 ± 0.02 eV to 0.40 ± 0.02 eV going from 248 nm to 193 nm. There is no apparent dependence of the maximum observed translational energy on dissociation wavelength. The general shape of all the $P(E_T)$ distributions peaking near zero E_T suggests the photodissociation occurs by a statistical dissociation following internal conversion to the ground electronic state in the absence of a barrier.

No theoretical studies have explicitly discussed the photodissociation dynamics of the CH/CD loss channel, but our results are generally consistent with calculations[15,35-37,63] performed on the CH ($^2\Pi$) + acetylene reaction that all predict a barrierless initial addition. These studies predict that dissociation to CH and acetylene proceeds indirectly, either by isomerization to cycloprop-2-enyl (C_S $^2A'$) or HC-CH-CH (C_1 ^2A) followed by CH loss or by dissociation to CH and vinylidene, which then isomerizes to acetylene. Vereecken suggests[37] direct dissociation to CH and acetylene is possible, but does not elaborate on the reaction pathway. The $P(E_T)$ distributions we report are consistent with any of these pathways, and it should be noted that our detector cannot distinguish between acetylene and vinylidene.

C. $CD_3 + C_2$

The $CD_3 + C_2$ channel is the highest-lying channel investigated in this study. This channel does not appear in the mass distribution for 540 nm detachment and 248 nm dissociation as seen in Figure 3A, in agreement with the energetics illustrated in Figure 1. Some CD_3 loss is evident at 450 nm/248 nm in Figure 3B, and this must come from propynyl. However, no $P(E_T)$ distribution could be constructed owing to the very low value of $E_{T,\,max}$ (see Table 1) and the associated problems discussed in Section III. CD_3 loss is evident at both detachment energies in the 193 nm dissociation experiments. This channel is expected for the propynyl radicals present after 450 nm photodetachment. After 540 nm detachment, where only propargyl is present, this channel most likely occurs by isomerization from propargyl to propynyl over the easily accessible barrier shown in Figure 1.

Figure 8 (black) shows the $P(E_T)$ distribution for CD_3 loss from propynyl and similarly suggests a barrierless, statistical dissociation from a vibrationally excited ground state following

internal conversion. This mechanism agrees well with the calculated heats of reaction and formation,[15,36-38] but further experiments and calculations on the electronically excited states of propynyl are needed to determine what excited states are responsible for the absorption. The red curve in Figure 8 shows the $P(E_T)$ distribution resulting from 193 nm photodissociation of propargyl. The average E_T for propargyl and propynyl is 0.27 ± 0.02 eV and 0.37 ± 0.02 eV, respectively. The difference presumably reflects the greater amount of energy available from the higher lying propynyl isomer (see Figure 1 and Table 1).

To our knowledge, the results presented here represent the first experimental account of propynyl absorption in the UV region and the first observation of its dissociation products. These results suggest Eisfeld's calculations[28] overestimate the energy of the second electronic excited state by over 1 eV.

V. Conclusions

The photodissociation of the propargyl-d_3 and propynyl-d_3 radicals at 248 nm and 193 nm was studied using fast beam photofragment translational spectroscopy. In this experiment, the radicals were prepared by photodetachment of the corresponding anions, the resulting radicals were photodissociated, and the photofragments were collected and analyzed using a coincidence imaging detector. In the ion source, a mixture of propargyl and propynyl anions was produced; we were able to distinguish between them by photodetaching at 540 nm, where only propargyl was energetically accessible, and at 450 nm, where both radicals were accessible. At each dissociation wavelength, the primary photoproducts were identified and translational energy ($P(E_T)$) distributions were measured.

The observed dissociation channels were $D_2 + C_3D$, $CD + C_2D_2$, and $CD_3 + C_2$. The D atom loss channel, previously shown to be the dominant channel in propargyl photodissociation,[41] could not be seen in this experiment owing to the large disparity in product masses. D_2 loss was observed at 248 nm from both radicals. For this channel, the $P(E_T)$ distributions from propargyl and propynyl peaked at 0.4 eV and 0.7 eV, respectively, consistent with small exit barriers that were calculated previously.[38] At 193 nm, D_2 loss was also seen but the signal was too low to develop a $P(E_T)$ distribution. The propargyl radical underwent CD loss at both dissociation wavelengths and some CD_3 loss at 193 nm. CD_3 loss was seen from propynyl at both wavelengths. All $P(E_T)$ distributions for CD and CD_3 loss peaked very close to zero translational energy, consistent with dissociation on the ground state surface with no exit barrier relative to the separated products.

Our results represent the first study of propynyl photdissociation, and the first characterization of the CD and CD_3 loss channels from the primary photodissociation of propargyl. They offer further evidence that propargyl dissociates when excited at 248 nm, and show that propynyl has accessible electronic states at 248 and 193 nm. These conclusions are at variance with a recent theoretical study[28] of the propargyl and propynyl excited states, suggesting that additional calculations are warranted.

Acknowledgments

This work was supported by the Director, Office of Basic Energy Sciences, Chemical Sciences Division of the U.S. Department of Energy under contract No. DE AC02-05CH11231.

References

1 C. H. Wu and R. D. Kern, J. Phys. Chem. **91**, 6291 (1987).

2 I. Cherchneff and J. R. Barker, Astrophys. J. **394**, 703 (1992).

3 I. Cherchneff, J. R. Barker, and A. Tielens, Astrophys. J. **401**, 269 (1992).

4 C. L. Morter, S. K. Farhat, J. D. Adamson, G. P. Glass, and R. F. Curl, J. Phys. Chem. **98**, 7029 (1994).

5 C. Ochsenfeld, R. I. Kaiser, Y. T. Lee, A. G. Suits, and M. HeadGordon, J. Chem. Phys. **106**, 4141 (1997).

6 R. I. Kaiser, Chem. Rev. **102**, 1309 (2002).

7 R. I. Kaiser and A. M. Mebel, Int. Rev. Phys. Chem. **21**, 307 (2002).

8 B. R. Giri, H. Hippler, M. Olzmann, and A. N. Unterreiner, Phys. Chem. Chem. Phys. **5**, 4641 (2003).

9 J. A. Miller and S. J. Klippenstein, J. Phys. Chem. A **107**, 7783 (2003).

10 Y. Georgievskii, J. A. Miller, and S. J. Klippenstein, Phys. Chem. Chem. Phys. **9**, 4259 (2007).

11 E. H. Wilson, S. K. Atreya, and A. Coustenis, Journal of Geophysical Research-Planets **108** (2003).

12 P. Botschwina, R. Oswald, J. Flugge, and M. Horn, Zeitschrift Fur Physikalische Chemie-International Journal of Research in Physical Chemistry & Chemical Physics **188**, 29 (1995).

13 X. Krokidis, N. W. Moriarty, W. A. Lester, and M. Frenklach, Chem. Phys. Lett. **314**, 534 (1999).

14 J. A. W. Harkless and W. A. Lester, J. Chem. Phys. **113**, 2680 (2000).

15 S. E. Wheeler, K. A. Robertson, W. D. Allen, H. F. Schaefer, Y. J. Bomble, and J. F. Stanton, J. Phys. Chem. A **111**, 3819 (2007).

16 J. D. DeSain and C. A. Taatjes, J. Phys. Chem. A **107**, 4843 (2003).

17 K. Tanaka, Y. Sumiyoshi, Y. Ohshima, Y. Endo, and K. Kawaguchi, J. Chem. Phys. **107**, 2728 (1997).

18 K. Tanaka, T. Harada, K. Sakaguchi, K. Harada, and T. Tanaka, J. Chem. Phys. **103**, 6450 (1995).

19 L. Yuan, J. DeSain, and R. F. Curl, J. Mol. Spectrosc. **187**, 102 (1998).

20 J. M. Oakes and G. B. Ellison, J. Am. Chem. Soc. **105**, 2969 (1983).

21 M. S. Robinson, M. L. Polak, V. M. Bierbaum, C. H. Depuy, and W. C. Lineberger, J. Am. Chem. Soc. **117**, 6766 (1995).

22 S. Ikuta, J. Mol. Struct. (Theochem) **434**, 121 (1998).

23 B. S. Jursic, J. Mol. Struct. (Theochem) **505**, 233 (2000).

24 R. K. Sreeruttun, P. Ramasami, G. Yan, C. S. Wannere, P. V. Schleyer, and H. F. Schaefer, Int. J. Mass. Spectrom. **241**, 295 (2005).

25 F. P. Lossing, Can. J. Chem. **50**, 3973 (1972).

26 D. W. Minsek and P. Chen, J. Phys. Chem. **94**, 8399 (1990).

27 T. Gilbert, R. Pfab, I. Fischer, and P. Chen, J. Chem. Phys. **112**, 2575 (2000).

28 W. Eisfeld, Phys. Chem. Chem. Phys. **7**, 3924 (2005).

29 D. A. Ramsay and Thistlet.P, Can. J. Phys. **44**, 1381 (1966).

30 A. Fahr, P. Hassanzadeh, B. Laszlo, and R. E. Huie, Chem. Phys. **215**, 59 (1997).

31 A. Fahr and A. H. Laufer, J. Phys. Chem. A **109**, 2534 (2005).

32 H. Honjou, M. Yoshimine, and J. Pacansky, J. Phys. Chem. **91**, 4455 (1987).

33 P. Botschwina, R. Oswald, J. Flugge, and M. Horn, Z. Phys. Chem. **188**, 29 (1995).

34 W. Eisfeld, J. Phys. Chem. A **110**, 3903 (2006).

35 R. Guadagnini, G. C. Schatz, and S. P. Walch, J. Phys. Chem. A **102**, 5857 (1998).

36 A. M. Mebel, W. M. Jackson, A. H. H. Chang, and S. H. Lin, J. Am. Chem. Soc. **120**, 5751 (1998).

37 L. Vereecken, K. Pierloot, and J. Peeters, J. Chem. Phys. **108**, 1068 (1998).

38 T. L. Nguyen, A. M. Mebel, and R. I. Kaiser, J. Phys. Chem. A **105**, 3284 (2001).

39 W. M. Jackson, D. S. Anex, R. E. Continetti, B. A. Balko, and Y. T. Lee, J. Chem. Phys. **95**, 7327 (1991).

40 H. J. Deyerl, I. Fischer, and P. Chen, J. Chem. Phys. **111**, 3441 (1999).

41 S. J. Goncher, D. T. Moore, N. E. Sveum, and D. M. Neumark, J. Chem. Phys. **128** (2008).

42 L. R. McCunn, B. L. FitzPatrick, M. J. Krisch, L. J. Butler, C. W. Liang, and J. J. Lin, J. Chem. Phys. **125** (2006).

43 T. L. Nguyen, A. M. Mebel, S. H. Lin, and R. I. Kaiser, J. Phys. Chem. A **105**, 11549 (2001).

44 P. Kebarle, J. Chem. Phys. **39**, 2218 (1963).

45 S. Satyapal and R. Bersohn, J. Phys. Chem. **95**, 8004 (1991).

46 K. Seki and H. Okabe, J. Phys. Chem. **96**, 3345 (1992).

47 W. Z. Sun, K. Yokoyama, J. C. Robinson, A. G. Suits, and D. M. Neumark, J. Chem. Phys. **110**, 4363 (1999).

48 X. Chen, Y. Ganot, I. Bar, and S. Rosenwaks, J. Chem. Phys. **113**, 5134 (2000).

49 S. Harich, J. J. Lin, Y. T. Lee, and X. Yang, J. Chem. Phys. **112**, 6656 (2000).

50 R. H. Qadiri, E. J. Feltham, E. E. H. Cottrill, N. Taniguchi, and M. N. R. Ashfold, J. Chem. Phys. **116**, 906 (2002).

51 R. H. Qadiri, E. J. Feltham, N. H. Nahler, R. P. Garcia, and M. N. R. Ashfold, J. Chem. Phys. **119**, 12842 (2003).

52 Y. Ganot, S. Rosenwaks, and I. Bar, J. Chem. Phys. **120**, 8600 (2004).

53 J. C. Robinson, N. E. Sveum, S. J. Goncher, and D. M. Neumark, Mol. Phys. **103**, 1765 (2005).

54 J. Zhou, E. Garand, W. Eisfeld, and D. M. Neumark, J. Chem. Phys. **127** (2007).

55 R. E. Continetti, D. R. Cyr, R. B. Metz, and D. M. Neumark, Chem. Phys. Lett. **182**, 406 (1991).

56 A. A. Hoops, J. R. Gascooke, A. E. Faulhaber, K. E. Kautzman, and D. M. Neumark, Chem. Phys. Lett. **374**, 235 (2003).

57 A. A. Hoops, J. R. Gascooke, K. E. Kautzman, A. E. Faulhaber, and D. M. Neumark, J. Chem. Phys. **120**, 8494 (2004).

58 K. S. Feldman and D. A. Mareska, Journal of Organic Chemistry **64**, 5650 (1999).

59 C. H. Depuy, V. M. Bierbaum, L. A. Flippin, J. J. Grabowski, G. K. King, and R. J. Schmitt, J. Am. Chem. Soc. **101**, 6443 (1979).

60 J. M. B. Bakker, J. Phys. E **6**, 785 (1973).

61 J. M. B. Bakker, J. Phys. E **7**, 364 (1974).

62 R. E. Continetti, D. R. Cyr, D. L. Osborn, D. J. Leahy, and D. M. Neumark, J. Chem. Phys. **99**, 2616 (1993).

63 S. P. Walch, J. Chem. Phys. **103**, 7064 (1995).

Table 1

$E_{T,\,max}$ (eV)	$D_2 + C_3D$		$CD + C_2D_2$		$CD_3 + C_2$	
	D_2CCCD	D_3CCC	D_2CCCD	D_3CCC	D_2CCCD	D_3CCC
λ_{diss} = 248 nm	2.2	2.9	1.1	1.8	0.0	0.1
λ_{diss} = 193 nm	3.6	4.3	2.5	3.3	0.8	1.5

Caption

Table 1: Table of maximum energy available for translation for each product channel from each isomer at each dissociation laser wavelength.

Captions

Figure 1: Energy level diagram of the propargyl (H_2CCCH) and propynyl (H_3CCC) radicals, their anions, and the accessible dissociation channels. The red (blue) arrows represent the energy available at 248 nm (193 nm). The dashed arrows represent the additional energy available for propargyl from photodetachment (see text).

Figure 2: Photodetachment efficiency curve as a function of photon energy in eV. The bold vertical line marks the electron affinity of the propynyl radical.

Figure 3: Mass distributions for photodissociation of C_3D_3 radicals at 248 nm. The top figure (A) features the photofragment masses after photodetachment of C_3D_3 anions at 540 nm, below the EA of propynyl. The bottom figure (B) features photofragment masses at 450 nm, above the propynyl EA.

Figure 4: Mass distributions for photodissociation of C_3D_3 radicals at 193 nm. The top figure (A) features the photofragment masses after photodetachment of C_3D_3 anions at 540 nm, below the EA of propynyl. The bottom figure (B) features photofragment masses at 450 nm, above the propynyl EA.

Figure 5: Comparison of the $P(E_T)$ distribution produced by the raw data with the 6 mm radius center discriminated (black) and the $P(E_T)$ distribution produced by normalizing the same data with the detector acceptance function (red).

Figure 6: (A) $P(E_T)$ distributions for the D_2 loss channel at 248 nm. The 540 nm (450 nm) detachment distribution is in red (black). (B) Comparison of 540 nm detachment distribution (red) with the distribution constructed from forward convolution (Ref. 40).

Figure 7: $P(E_T)$ distributions for the CD loss channel. The distributions are pairwise compared holding photodetachment laser wavelength or photodissociation laser wavelength constant.

Figure 8: $P(E_T)$ distributions for the CD_3 loss channel at 193 nm. In red (black) is the distribution resulting from 540 nm (450 nm) photodetachment.

Figure 1

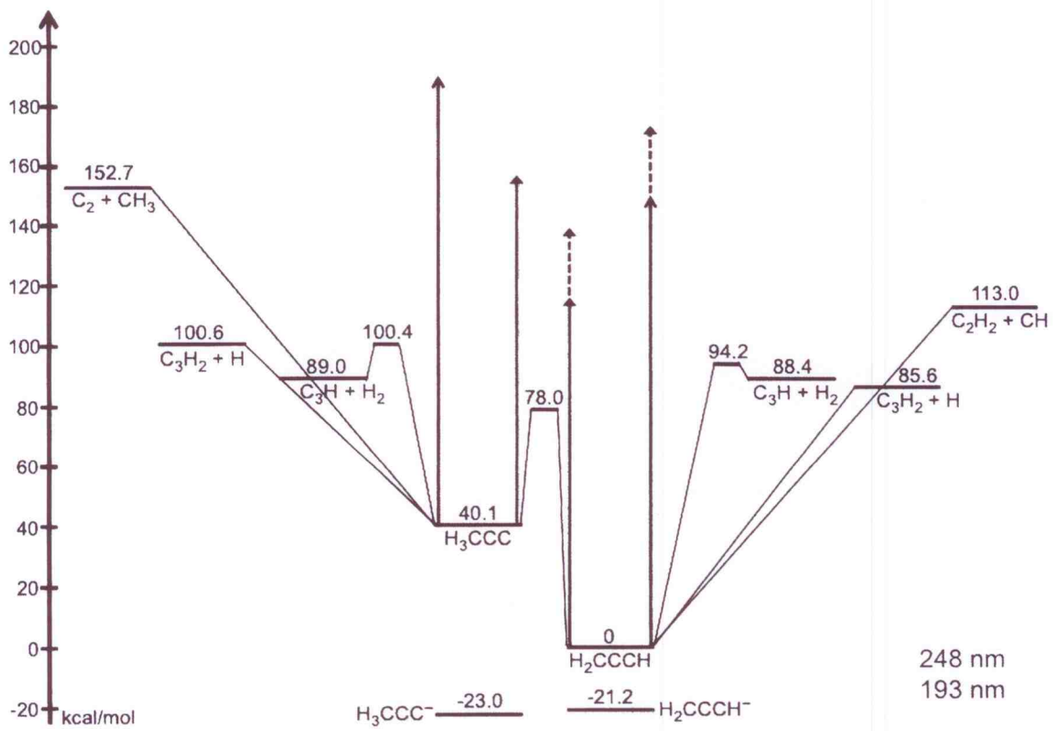

Figure 2

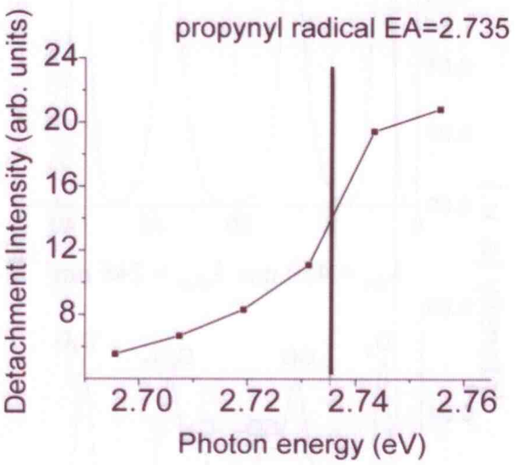
propynyl radical EA=2.735
Detachment Intensity (arb. units)
24
20
16
12
8
2.70
2.72
2.74
2.76
Photon energy (eV)

Figure 3

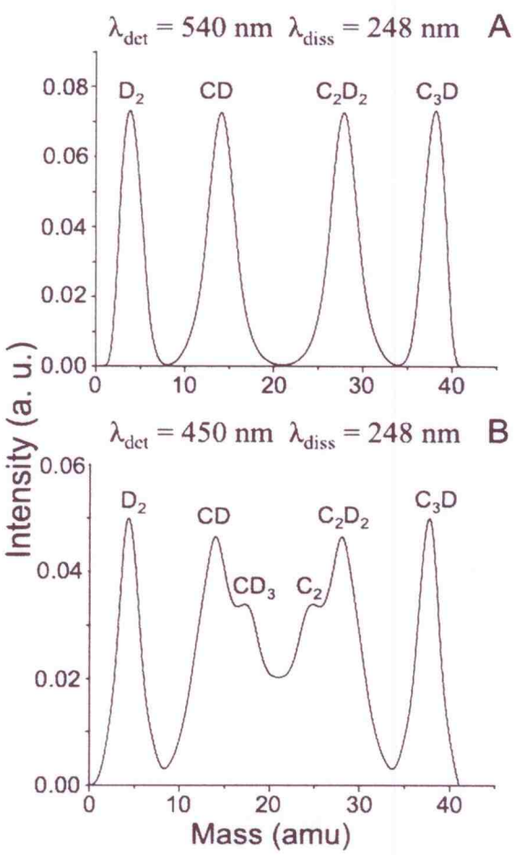
λdet = 540 nm λdiss = 248 nm A
D2
CD
C2D2
C3D
0.08
0.06
0.04
0.02
0.00
0
10
20
30
40
λdet = 450 nm λdiss = 248 nm B
D2
CD
CD3
C2
C2D2
C3D
0.06
0.04
0.02
0.00
Intensity (a. u.)
Mass (amu)

Figure 4

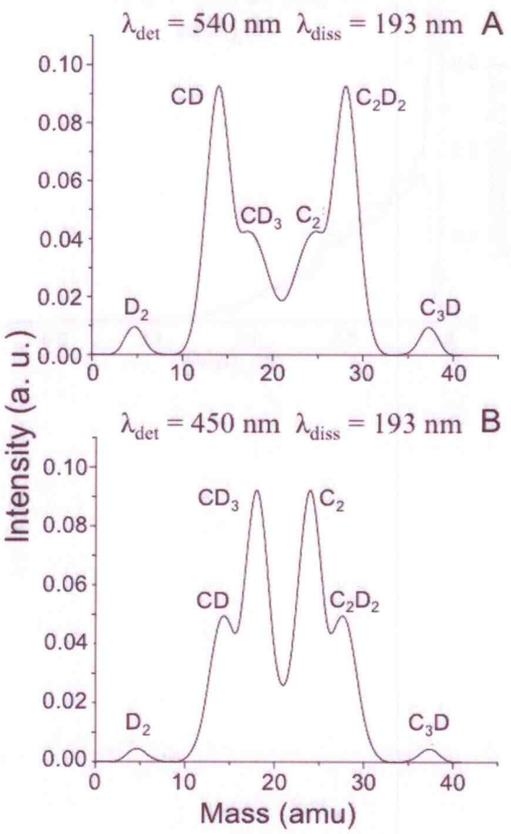
λdet = 540 nm λdiss = 193 nm A
CD
C2D2
CD3
C2
D2
C3D
λdet = 450 nm λdiss = 193 nm B
CD3
C2
CD
C2D2
D2
C3D
Intensity (a. u.)
Mass (amu)
0.00
0.02
0.04
0.06
0.08
0.10
0
10
20
30
40

Figure 5

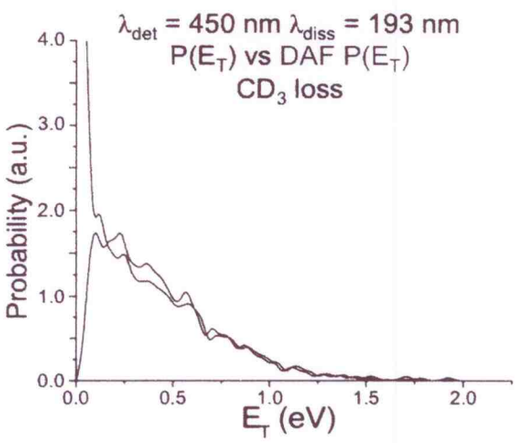
λ_{det} = 450 nm λ_{diss} = 193 nm
P(E_T) vs DAF P(E_T)
CD_3 loss
Probability (a.u.)
4.0
3.0
2.0
1.0
0.0
0.0
0.5
1.0
1.5
2.0
E_T (eV)

Figure 6

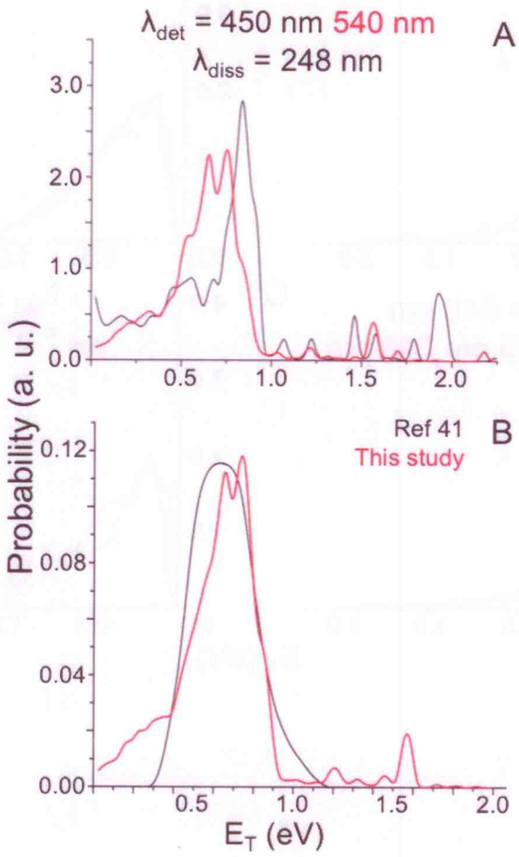
λdet = 450 nm 540 nm
λdiss = 248 nm
A
3.0
2.0
1.0
0.0
0.5
1.0
1.5
2.0
Ref 41
This study
B
Probability (a. u.)
0.12
0.08
0.04
0.00
0.5
1.0
1.5
2.0
ET (eV)

Figure 7

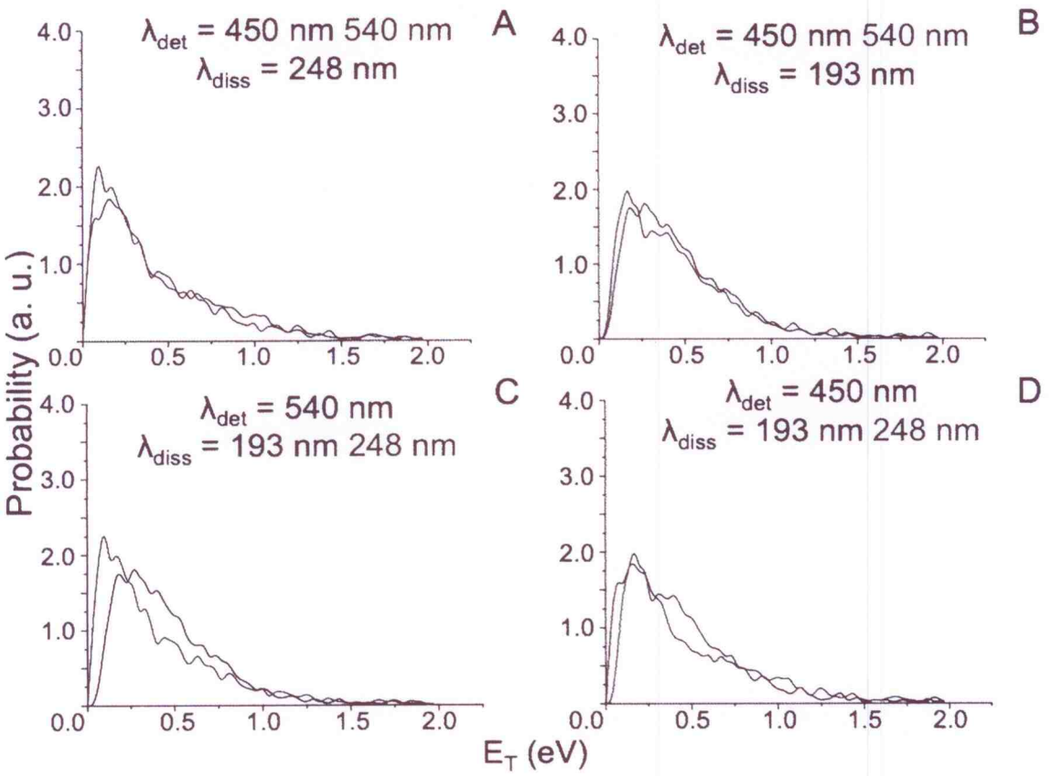

Figure 8

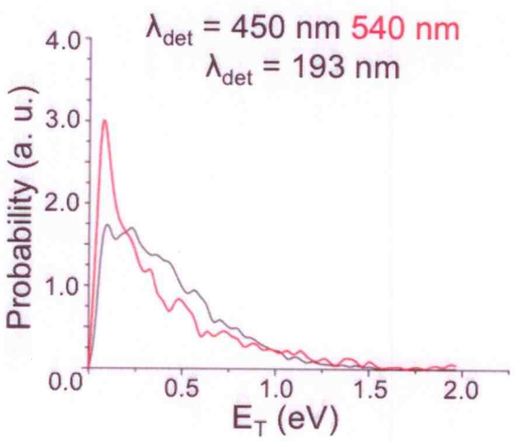
λdet = 450 nm 540 nm
λdet = 193 nm
Probability (a. u.)
4.0
3.0
2.0
1.0
0.0
0.5
1.0
1.5
2.0
ET (eV)